Instruments and Methods

Seismic wave attenuation in the uppermost glacier ice of Storglaciären, Sweden

Alessio GUSMEROLI,[1] Roger A. CLARK,[2] Tavi MURRAY,[1] Adam D. BOOTH,[1] Bernd KULESSA,[1] Brian E. BARRETT[3]

[1] *School of the Environment and Society, Swansea University, Singleton Park, Swansea SA2 8PP, UK*
E-mail: 393446@swansea.ac.uk
[2] *School of Earth and Environment, University of Leeds, Woodhouse Lane, Leeds LS2 9JT, UK*
[3] *Zetica Ltd, Units 15/16 Hanborough Business Park, Long Hanborough, Oxfordshire OX29 8LH, UK*

ABSTRACT. We conducted seismic refraction surveys in the upper ablation area of Storglaciären, a small valley glacier located in Swedish Lapland. We estimated seismic-wave attenuation using the spectral-ratio method on the energy travelling in the uppermost ice with an average temperature of approximately –1°C. Attenuation values were derived between 100 and 300 Hz using the P-wave quality factor, Q_P, the inverse of the internal friction. By assuming constant attenuation along the seismic line we obtained mean $Q_P = 6 \pm 1$. We also observed that Q_P varies from 8 ± 1 to 5 ± 1 from the near-offset to the far-offset region of the line, respectively. Since the wave propagates deeper at far offsets, this variation is interpreted by considering the temperature profile of the study area; far-offset arrivals sampled warmer and thus more-attenuative ice. Our estimates are considerably lower than those reported for field studies in polar ice (~500–1700 at –28°C and 50–160 at –10°C) and, hence, are supportive of laboratory experiments that show attenuation increases with rising ice temperature. Our results provide new in situ estimates of Q_P for glacier ice and demonstrate a valuable method for future investigations in both alpine and polar ice.

INTRODUCTION

Recent developments in glacier-flow modelling have highlighted the necessity of including ice liquid-water content within the model input parameters (Hubbard and others, 2003; Chandler and others, 2008). This is because the presence of free water at the intergranular scale greatly softens temperate glacier ice and, consequently, strongly increases its deformation rate (Duval, 1977). Since direct sampling of ice water content is logistically challenging, and often fails to correctly reproduce a sample's boundary conditions (e.g. temperature and confining pressure), efforts have been made recently (Barrett and others, 2007; Murray and others, 2007; Gusmeroli and others, 2008; Bradford and others, 2009; Endres and others, 2009) to constrain ice water content using in situ geophysical techniques.

The vast majority of published works on glacier ice water content consider the influence that water content has on the propagation speed of geophysical signals such as electromagnetic (Macheret and others, 1993; Murray and others, 2000; Bradford and Harper, 2005) and elastic (Benjumea and others, 2003; Navarro and others, 2005) waves. Endres and others (2009) showed that by jointly inverting spatially coincident radar and seismic wave speeds it is possible to obtain physically consistent water-content and pore geometry estimates for a two-phase (ice/water) medium. However, since air bodies in the form of bubbles, englacial voids and fractures are commonly observed in glaciers (Pohjola, 1994), this interpretation is non-unique (Bradford and Harper, 2005; Gusmeroli and others, 2008). A three-phase model should be considered in order to estimate the volumetric content and geometry of both air and water inclusions within glacier ice. As an example, relatively high electromagnetic (and low seismic) speeds could be indicative of either dry, bubble-free or wet, bubbly glacier ice.

A few workers (Macheret and Glazovsky, 2000; Bradford and others, 2009) include the presence of air bubbles in their water-content estimates. However, since these procedures do not consider electromagnetic wave speed being influenced by air-rich features (e.g. fractures and englacial voids), it is desirable that additional parameters, other than speed, are included in the analysis to obtain more reliable water-content estimates. These parameters, rarely measured in glaciers, are radar and seismic attenuation (Endres and others, 2009); the combined use of radar and seismic speeds with corresponding attenuations would provide sufficient parameters to estimate the volumetric content and geometry of both air and water inclusions within glacier ice. In fact, since propagation properties (speed and attenuation) of geophysical signals are sensitive to water, four independent parameters, jointly inverted, (instead of two) clearly add to the aim of describing glacier-ice properties using radar and seismic surveys.

Furthermore, values of seismic attenuation are routinely used when exploring subglacial properties using seismic surveys (Smith, 1997, 2007; King and others, 2008; Peters and others, 2008), and uncertainties in these values often constitute limitations in the techniques used to derive bed properties (Smith, 2007). Here we apply current methods from hydrocarbon exploration (Tonn, 1991; Dasgupta and Clark, 1998) to estimate P-wave seismic attenuation within the polythermal glacier Storglaciären, Swedish Lapland, and hence demonstrate a methodology which can form the basis

https://doi.org/10.3189/002214310791968485 Published online by Cambridge University Press

Table 1. Examples of Q_P estimates in polar and alpine ice masses from previous studies. FD and FI indicate frequency-dependent (FD) and frequency-independent (FI) Q and α

Study	Location	Temperature °C	Q_P	Methodology	f Hz
Westphal (1965)	Blue Glacier, Washington, USA	~0	129–172*	FDα	25 000
Clee and others (1969)	Athabasca Glacier, Canada	~0	65	FDα–FIQ	120–1000
Bentley and Kohnen (1976)	Byrd Station, Antarctica	−28	526–1667	FDQ	136
Jarvis and King (1993)	Larsen Ice Shelf, Antarctica	−10 to −12†	50–160*	FIα	100–300‡

*Recalculated from published α using Equation (1).
†Temperature from Reynolds (1981), Vaughan and Doake (1996) and Smith (1997).
‡Recalculated from α in this frequency range to facilitate comparison with our study.

for future development in this important and rarely explored aspect of seismic-wave propagation in glaciers.

The seismic quality factor, Q

The attenuation of seismic energy is usually quantified using the non-dimensional seismic quality factor, Q, or its inverse, Q^{-1}, the internal friction. Q is a fundamental property of rocks and Earth materials, and is defined by the fractional energy loss per cycle experienced by a propagating seismic wave (Knopoff, 1964; Toksöz and Johnston, 1981; Sheriff and Geldart, 1995). High Q values (500–1000) are expected for non-attenuative materials such as massive crystalline rocks, and low Q values (10–100) are typical for attenuative materials such as porous and/or fractured rocks. There are many definitions of Q in the seismological literature; in this study we use the one provided by Aki and Richards (2002), the definition typically used in glaciological studies (e.g. Clee and others, 1969; Bentley and Kohnen, 1976):

$$Q = \frac{\pi f}{\alpha v}, \tag{1}$$

where f, v and α are frequency, propagation speed and attenuation coefficient, respectively. Q values in frozen rocks are very much higher than those observed in unfrozen rocks (Spetzler and Anderson, 1968; Toksöz and others, 1979). The degree of water saturation also influences seismic attenuation. In some cases, Q values are known to be similar for dry and fully saturated materials but are significantly lower for partial degrees of saturation (Winkler and Nur, 1982); in fact, partial saturation allows space for fluid squirt-flow (pressure-induced, intragranular fluid flow) between and within fractures, microcracks on grain surfaces, and pore spaces (Toms and others, 2007).

Only a few measurements of seismic attenuation are available in the glaciological literature. Comprehensive reviews of seismic-attenuation studies in polar ice are provided by Smith (1997, 2007). Some workers measure seismic attenuation using time-domain analysis of α (Robin, 1958; Westphal, 1965; Jarvis and King, 1993), whereas others (Clee and others, 1969; Bentley and Kohnen, 1976) use Q^{-1}. The results of this prior research show that the P-wave quality factor, Q_P, is generally higher for cold ice (Q_P ~500–1700 at Byrd Station, Antarctica; Bentley and Kohnen, 1976) than for temperate ice ($Q_P \sim 65$ at Athabasca Glacier, Canada; Clee and others, 1969). This evidence is also supported by Kuroiwa (1964), who conducted laboratory measurements of the internal friction in natural polycrystalline glacier ice. He observed that Q_P increases (attenuation decreases) from low values ($Q_P \sim 40$) near the melting point to very high values (Q_P up to 1000) around −30°C. Despite this, it is very difficult to obtain a clear range of Q_P estimates in glacier ice, since previous workers measure attenuation over different frequency ranges, using different methods, different equations and different assumptions. Table 1 shows a compilation of previous Q_P estimates (in some cases recalculated) from different glaciological settings.

In situ Q_P estimates are always made as effective attenuation, $1/Q_{\text{eff}}$, in the medium. These values are controlled by intrinsic effects (e.g. material properties) and also by apparent attenuation processes (e.g. scattering from inclusions, heterogeneities, rough interfaces and/or interference between direct arrivals and short-path multiples). Effective attenuation is related to intrinsic ($1/Q_{\text{int}}$) and apparent ($1/Q_{\text{app}}$) attenuation by (Spencer and others, 1982):

$$\frac{1}{Q_{\text{eff}}} = \frac{1}{Q_{\text{int}}} + \frac{1}{Q_{\text{app}}}. \tag{2}$$

Modelling (Dvorkin and Nur, 1993) and observations (Sams and others, 1997) of attenuation mechanisms show that seismic Q is frequency-dependent when considered over several orders of magnitude (e.g. 10^{-3} to 10^4 Hz). However, other studies suggest that the frequency dependence is negligible (Johnston and others, 1979). Here we apply the frequently used concept of frequency-independent Q (Mitchell, 1975; Johnston and others, 1979; Kjartansson, 1979; Dasgupta and Clark, 1998; Xia and others, 2002; Wang, 2003; Reine and others, 2009), and our Q estimates are assumed to be constant within the measurement bandwidth.

METHODS

Seismic attenuation and the spectral-ratio method

Following the fundamental principles that control seismic-wave attenuation and dispersion (Futterman, 1962) for the specific case of frequency-independent Q, we can describe the change in amplitude spectrum from A_0 to A_1 after travelling a distance, x, using the frequency-dependent attenuation coefficient, α (Aki and Richards, 2002):

$$A_1 = GRA_0 e^{-\alpha x}, \tag{3}$$

where G and R are, respectively, the geometric spreading factor and the energy partitioning at interfaces (when the wave crosses a boundary between two media); these two

https://doi.org/10.3189/002214310791968485 Published online by Cambridge University Press

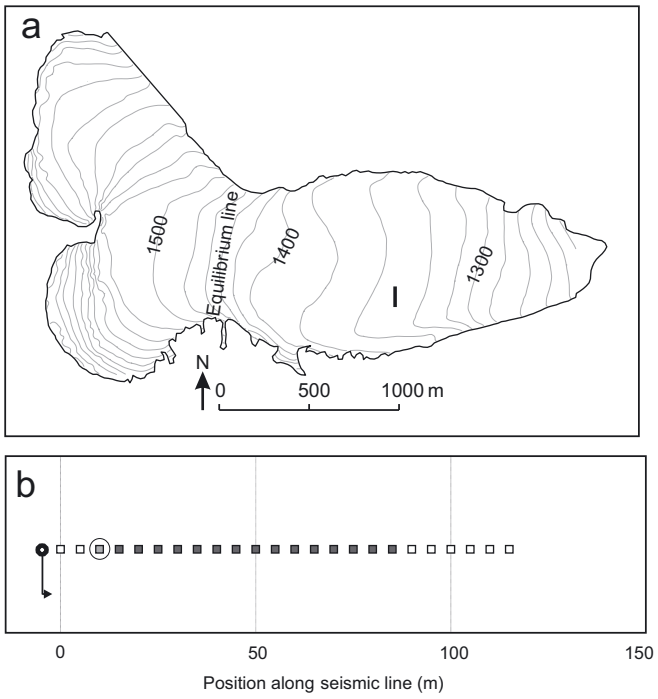

Fig. 1. (a) Location of the seismic line at Storglaciären (67°90′N, 18°57′E). Surface elevation in metres above sea level. (b) Schematic of the survey. The black circle indicates the shot position; white and filled squares indicate unused and used geophones, respectively. The arrow indicates the direction of the P-wave sampled. The circled geophone, located at 15 m from the source, was used as the reference arrival in the analysis (A_0 in Equation (5)).

terms are treated as frequency-independent. Considering Equation (1), Equation (3) becomes:

$$A_1 = GRA_0 e^{-\frac{\pi f}{vQ}x}. \quad (4)$$

This equation provides the theoretical basis of the spectral-ratio method, a popular method of obtaining frequency-independent Q estimates from field datasets, such as vertical seismic profiles (Tonn, 1991; Wang, 2003) and surface-reflection surveys (Dasgupta and Clark, 1998; Reine and others, 2009).

Equation (4) implies higher frequencies are preferentially attenuated. In this instance, the natural logarithm of the ratio between the attenuated and non-attenuated amplitude is (for constant Q and v) a linear function of frequency (Tonn, 1991):

$$\ln\left(\frac{A_1}{A_0}\right) = -\frac{\pi f}{Qv}x + c, \quad (5)$$

Table 2. Details of the seismic surveys used in the Q_P analysis at Storglaciären

Shot	Date	Time
		h
SG6j	6 July 2008	1549
SG7j-1	7 July 2008	1117
SG7j-2	7 July 2008	1624

where c is $\ln(GR)$ and contains all frequency-independent terms. Equation (5) shows $\ln(A_1/A_0)$ is linear in frequency, with a slope, γ, given by:

$$\gamma = -\frac{\pi \delta t}{Q}. \quad (6)$$

In typical experimental settings, the wavelet is sampled at two locations separated by a distance δx, and γ is converted to Q for the given $\delta t = \delta x/v$. When many pairs of attenuated signals are available, with a range of travel-time differences, all of them sampling a volume considered to be characterized by a single Q, this Q can be derived from a linear regression of spectral-ratio slope, γ, against δt (which is directly estimated from the travel times):

$$Q = -\frac{\pi}{m}, \quad (7)$$

where m is the slope of the regression line. Assuming constant Q within the medium, a more robust result can be derived by sampling the waves at a higher number of locations; we exploit this intensive sampling approach here.

Field experiment

In July 2008 we conducted seismic surveys in the ablation area of Storglaciären (Fig. 1), a well-studied polythermal glacier located in Swedish Lapland. The ablation zone of the glacier has a cold-ice surface layer above a temperate core (Holmlund and Eriksson, 1989; Pettersson and others, 2003). At the time of the survey the glacier was snow-free and the seismic line was located near a thermistor string which provided temperature data in the uppermost 28 m of ice. Data were acquired using a hammer-and-plate source, and the receivers (24 geophones at 100 Hz) were positioned along a 115 m line, transverse to glacier flow, with 5 m spacing (see Fig. 1 for location and survey geometry). The distance between the source and closest geophone was 5 m. The seismic line (see Fig. 2 for data example) was repeated over 2 days at different times in order to detect any temporal variation (see Table 2 for details of the surveys).

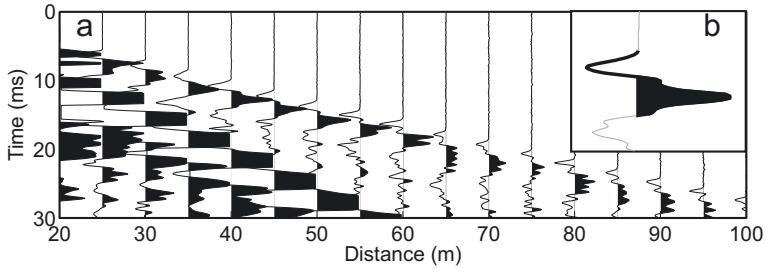

Fig. 2. Example of unprocessed seismograms used in the computation of Q_P. (a) Sample data from Storglaciären; the first arrivals are refractions propagating through the uppermost ice. (b) Extracted wavelet at 40 m offset.

https://doi.org/10.3189/002214310791968485 Published online by Cambridge University Press

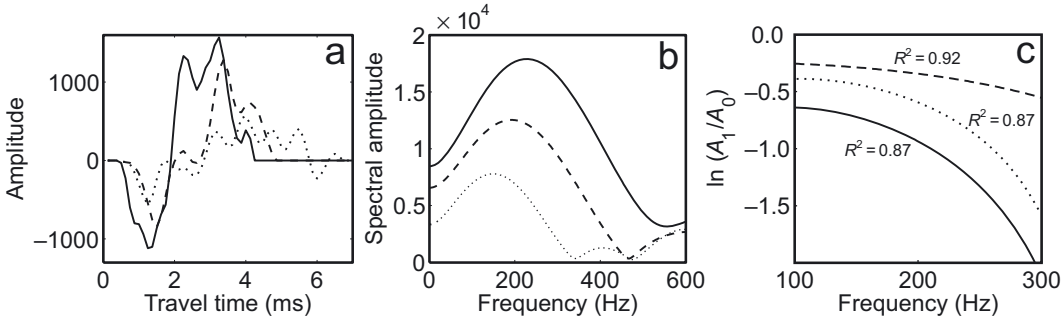

Fig. 3. (a) Examples of the time windows used to perform the spectral analysis for 25, 50 and 75 m offsets (solid, dashed and dotted curves, respectively). (b) Fourier spectra in the bandwidth 0–600 Hz of the three sample arrivals. (c) Natural logarithm of the spectral ratio in the bandwidth 100–200 Hz for the pairs of offsets 75/25, 50/25 and 75/50 m (solid, dashed and dotted curves, respectively).

We undertook seismic-attenuation analyses on refractions travelling in the uppermost ice layer. Examples of the consecutive processing steps used are given in Figure 3. From each arrival we manually extracted the first cycle of the wavelet using a cosine-tapered time window with a plateau from the first break of the arrival to its second subsequent zero crossing (Fig. 2b). The full window length (Fig. 3a) used to obtain the Fourier spectra (Fig. 3b) included a taper before and after the plateau; the length of the taper was 10% of the length of the first cycle. The natural logarithms of the spectral ratios (e.g. Figs 3c and 4) between the reference wavelet (arbitrarily picked as 15 m offset from the source; Fig. 1b) and the arrivals recorded at 15 subsequent geophones were then computed and plotted as a function of frequency to derive the slope of the ln(spectral ratio), γ, which, according to Equation (6), is a function of Q and the travel time between the two arrivals. Longer offsets showed poor signal-to-noise ratios, so were not used.

In this process, the selection of the bandwidth is critical, since the spectral ratios are representative of Q only in the region of the spectra where there is energy. In our data we chose to derive Q in a bandwidth of 100–300 Hz, where the energy spectrum is highest even for far-offset arrivals (Fig. 3b). As shown in Figure 3b, the spectrum for the longest offset considered (75 m) is mostly concentrated in this bandwidth and decreases rapidly at frequencies higher than 300 Hz.

RESULTS

The key parameter used in the determination of Q_P is γ, the slope of the regression line which relates the linear decay to the frequency of the spectral ratios between two arrivals separated by travel time, δt (Equations (5) and (6)). Errors in our γ estimates are typically low, since the correlation between ln(spectral ratio) and frequency is generally good (Figs 3c and 4). Deviations from a linear relationship in the spectral ratios provide evidence of frequency dependence of Q_P, which is discussed below. Figure 5 shows how γ decreases in the three shots as δt increases; this behaviour is a function of Q_P. General agreement between the three shots is observed. Assuming constant attenuation along the seismic line and simply fitting a straight line to the γ vs δt pairs, in all three experiments we obtain a similar mean m (Equation (7)), which corresponds to $Q_P = 6 \pm 1$ (Fig. 5a).

This average value gives a useful indication of the high seismic attenuation generally observed in our data, but is not the only way to interpret the results. In fact, when we observe all the data points in Figure 5, clear breaks in slope (Fig. 5b–d) suggest that Q_P decreases at high δt. We identify two regions of different slope, one at low/central δt (which

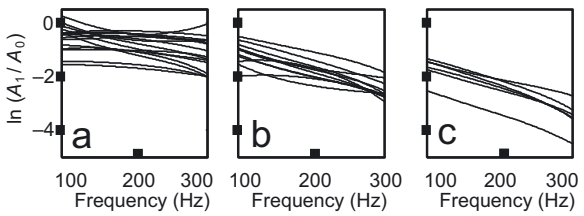

Fig. 4. Representative examples of spectral ratios for different receiver separation, δx. (a) $\delta x = 25$ m, $\delta t = 0.007$ s; (b) $\delta x = 50$ m, $\delta t = 0.014$ s; (c) $\delta x = 75$ m, $\delta t = 0.021$ s.

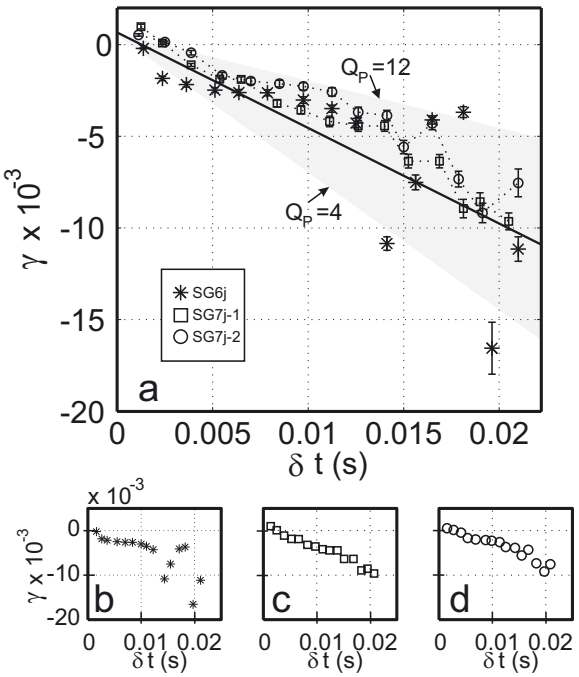

Fig. 5. Plots of γ vs δt used in the Q_P estimates at Storglaciären. (a) Results for the three shots. The solid line indicates the best straight-fit line obtained from the mean m in the three shots, which gives $Q_P = 6 \pm 1$. The area marked in grey is bounded by two straight lines describing the highest and lowest Q_P observed at SG (12 and 4 respectively). Three single shots are shown for clarity in (b), (c) and (d). Symbols shown in (a) are also used in (b), (c) and (d). Details of the different shots are given in Table 2.

https://doi.org/10.3189/002214310791968485 Published online by Cambridge University Press

Table 3. Estimates of Q_P for the uppermost ice at Storglaciären. Parenthetical 'all', '20–65' and '65–90' indicate the portion of the line considered in the analysis. R^2 values are also given

Shot	Q_P(all)	R^2(all)	Q_P(20–65)	R^2(20–65)	Q_P(65–90)	R^2(65–90)
SG6j	6 ± 2	0.58	6 ± 2	0.62	6 ± 7	0.12
SG7j-1	6 ± 1	0.97	7 ± 1	0.94	4 ± 1	0.91
SG7j-2	7 ± 1	0.91	9 ± 1	0.92	5 ± 1	0.72

corresponds to geophones positioned between 20 and 65 m) with higher Q_P (~8), and a second region at high δt (65–90 m) with Q_P as low as 4. Results of the Q_P computation using all the receiver pairs and dividing the data points into two regions are listed in Table 3. R^2 values are typically high, except at high δt in SG6j (Fig. 5a and b), where the accuracy appears to be low (probably noisy data points due to poor geophone coupling).

The results listed in Table 3 were calculated with Equation (5), using the amplitude recorded in the receiver located at 15 m offset as A_0. We can also investigate potential changes in Q_P values using different receivers as the reference. Figure 6 shows that m and Q_P, for a given range of A_1, are the same, even when different geophones are used. The only differences generated by changing the reference geophone are changes in intercept. Q_P is higher (~9) at low/central δt and is clearly lower (~5) at higher travel times (Fig. 6).

The measurement error associated with m was calculated using the standard error of the regression line. Errors in m, ϵ_m, were then converted to errors in Q_P, ϵ_{Q_P}, combining Equation (7) with the standard equations for error propagation (e.g. Topping, 1972); these equations are commonly used to calculate the error of compound quantities:

$$\epsilon_{Q_P} = -\frac{\pi \epsilon_m}{m^2}. \quad (8)$$

Errors in Q_P are generally low in all our experiments (Table 3) except at high δt in SG6j ($Q_P = 6 \pm 7$).

DISCUSSION

Seismic attenuation and ice temperature. Are our estimates reasonable?

The first issue that needs to be addressed from our results in Table 3 is that these values are strikingly low compared to published examples for glacier ice (Table 1). As mentioned in the introduction, there is much evidence supporting a strong temperature dependence of Q_P in glacier ice (Kuroiwa, 1964; Clee and others, 1969; Bentley and Kohnen, 1976; Jarvis and King, 1993). It is therefore reasonable to consider particularly high Q_P (as measured at Byrd Station by Bentley and Kohnen, 1976) to be typical of glacier ice substantially colder than the melting point (average temperature −28°C). Jarvis and King (1993) reported much higher attenuation at the more northerly (thus warmer) Larsen Ice Shelf (ice temperature around −10°C; Reynolds, 1981; Vaughan and Doake, 1996).

The central value given by Bentley and Kohnen (1976) is $Q_P = 714$ at 136 Hz; deriving Q_P from α (Equation (1)) for the Jarvis and King (1993) value gives $Q_P = 68$ at 136 Hz. Thus, the seismic quality factor appears to be more than ten times higher if ice temperature is increased by ~18°C. Estimates in temperate ice (Westphal, 1965; Clee and others, 1969) are not easy to compare since they have been derived for much higher frequencies (kHz) than those reported by Bentley and Kohnen (1976) and Jarvis and King (1993) and used in the work presented here.

The temperature profile with depth from a thermistor string adjacent to the seismic line is shown in Figure 7. Temperature data were collected and processed as described by Pettersson and others (2004). At this location, Storglaciären is polythermal with a 20 m thick cold surface layer (lowest temperature about −1.5°C) underlain by temperate ice. The temperature profile is particularly important in the interpretation of our estimates, but the interpretation is not straightforward. What ice temperature do our Q_P estimates relate to? What depth is sampled by the propagating P-wave?

One way to answer these questions is by looking at the Fresnel volume: the finite volume of space around the geometric ray path that influences the propagation of a band-limited wave (Spetzler and Snieder, 2004). Thus the maximum depth, q, sampled by a propagating P-wave is the radii of the Fresnel volume given by Spetzler and Snieder (2004) as:

$$q = \sqrt{\frac{3}{4}\frac{\lambda(x/2)^2}{x}}, \quad (9)$$

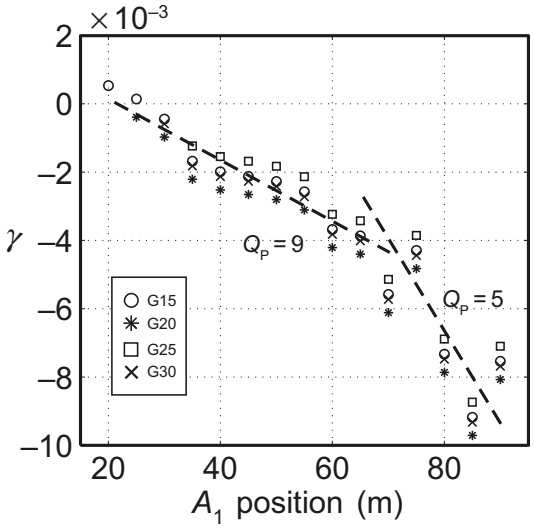

Fig. 6. Plot of γ vs δt for SG7j-2 using different geophones as reference signal, A_0 in Equation (5). Changes in slope, m (and thus Q_P), are consistent along the seismic line even when different geophones are used. Changes in intercept are probably due to changes in the absolute amplitude of arrivals recorded at different geophones. Different symbols are for different reference geophones. G15, G20, G25 and G30 indicate that the reference arrival has been extracted from the geophone located at 15, 20, 25 and 30 m, respectively.

https://doi.org/10.3189/002214310791968485 Published online by Cambridge University Press

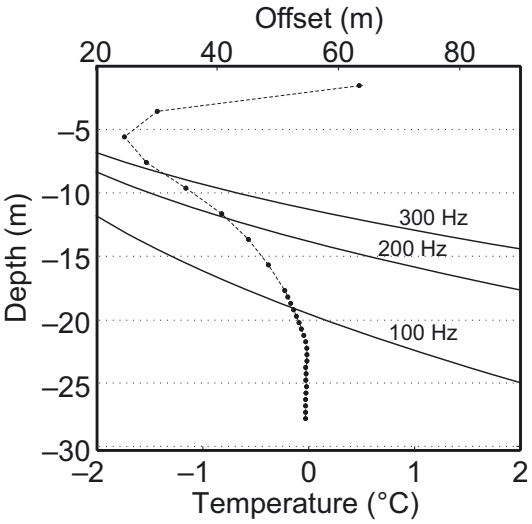

Fig. 7. Temperature profile with depth (dots, dashed curve) from the thermistor string located where the seismic line was acquired at Storglaciären. The maximum size of the radii of the first Fresnel volume (thus the depth sampled by the ray path) calculated using Equation (9) is shown as black, solid lines. The Fresnel volume is frequency-dependent, and the frequencies used in our seismic-attenuation analysis (100, 200 and 300 Hz) are shown. Temperature and Fresnel volume depth are plotted on the same graph to show how higher offsets are sampling warmer ice.

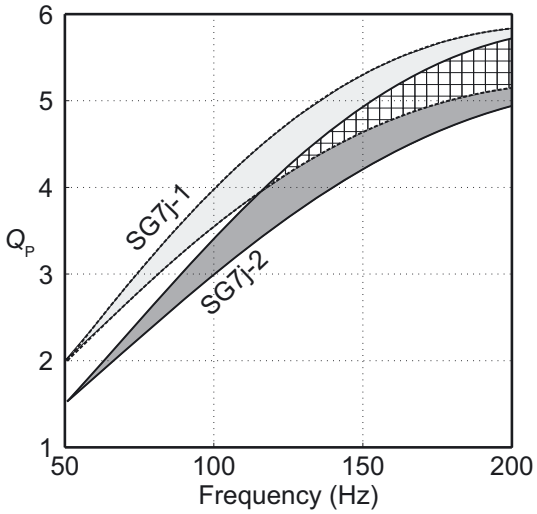

Fig. 8. Attenuation spectrum for frequency-dependent Q_P, computed using the spectral ratios and the method of Jeng and others (1999). Only two shots are shown for clarity. Light and dark grey areas indicate the uncertainty in SG7j-1 and SG7j-2, respectively. The hatched area is common for both shots.

where λ and x are wavelength and offset, respectively. Figure 7 shows the depth of the first Fresnel volume superimposed on the temperature profile for the bandwidth used in our study. The Fresnel volume increases with offset, changing from 12 to 25 m for 100 Hz energy. It is therefore likely that far-offset receivers sampled a wave which propagated in warmer ice than the one sampled by near-offset receivers. Thus, if we define the maximum effective depth as that sampled by the lowest frequency (100 Hz) we can conclude that differences in m and Q_P observed in Figures 5 and 6 are probably due to the fact that earlier arrivals propagate principally in cold ice (with temperature around -1°C; Fig. 7) whereas at higher δt the low Q_P values are generated by a wave propagating in warmer ice, probably, at least partially, in the temperate ice.

Frequency-dependent Q and temporal variations

The methodology applied in this study appears to be an efficient tool for monitoring the thermal state of glaciers using frequency-independent Q_P estimates. The advantage of the frequency-independent estimate is that we have quantified the variability in time of a number of values of γ, estimated in the frequency domain; since the wave propagates deeper at high δt, we observed temperature-related variations in our frequency-independent Q_P estimates. Despite this, the deviations from linear in Figures 3c and 4 indicate there is some frequency dependence of Q_P. We therefore provide an example of the calculation of Q_P when it is assumed to be frequency-dependent (and thus time-independent). We apply the method suggested by Jeng and others (1999): for each frequency we take the natural logarithm of the amplitude ratio $A_1(f)/A_0(f)$, and plot it against δt. The slope of the regression line is $\pi f/Q$ which gives Q for that frequency (see Equation (5)).

Figure 8 shows the spectrum of Q_P in the frequency range 50–200 Hz for the two shots collected on 7 July. Absolute Q_P values seem slightly lower for the morning shot (SG7j-1) than the afternoon one (SG7-2). We can use this plot to obtain a single, frequency-independent estimate of the attenuation coefficient, α, using Equation (1). A linear regression in Figure 8 is in the form $Q = (\pi/\alpha v)f$. Thus α is derived using the slope of the line in Figure 8. This simple, though crude, calculation gives $\alpha = (3.47 \pm 0.68) \times 10^{-2}$ and $(3.14 \pm 0.68) \times 10^{-2}$ m^{-1} for SG7j-1 and SG7j-2, respectively. These values are ~15 and ~150 times higher than those reported by Jarvis and King (1993) and Bentley and Kohnen (1976), respectively; this is further evidence that seismic attenuation is much higher in valley glaciers whose temperature is close to the melting point than in polar ice masses.

Temporal variations in Q_P, or general seismic attenuation, are neglected in our analysis. Although the survey conditions may have changed between the morning (low melt rate) and the afternoon (high melt rate), we did not find any significant variations in our estimates. In fact, as discussed in the previous section, the depth of ice sampled by our data is probably insensitive to surface variations. Minor exceptions include the anomalies observed at high δt in SG6j (Fig. 5b) and the slightly higher Q_P for the morning shot in the frequency-dependent calculation (Fig. 8). We believe that these are insufficient to confirm temporal Q_P variations; nonetheless we recognize that understanding temporal variations (e.g. hydrologically forced) of Q_P could be an exciting way to improve our understanding of the relationship between seismic attenuation and other ice properties, such as temperature and water content.

CONCLUSIONS AND OUTLOOK

Seismic-refraction surveys have been carried out in the upper ablation area of Storglaciären in order to estimate seismic P-wave attenuation using the quality factor, Q_P. A methodology, based on the spectral-ratio method, has been tested and is discussed in terms of its ability to offer new insights into the geophysical characterization of glacier ice properties. We have undertaken spectral analysis on

https://doi.org/10.3189/002214310791968485 Published online by Cambridge University Press

15 subsequent arrivals, covering a total geophone spread of 90 m. Results of this analysis show that average seismic attenuation in the uppermost 10–25 m of Storglaciären is very high ($Q_P \sim 6$), around 10 and 100 times higher than previously reported on the Larsen Ice Shelf (Jarvis and King, 1993) and at Byrd Station (Bentley and Kohnen, 1976), respectively. Such differences are explained by noting that the average ice temperature which influences our data is about −1°C, whereas it was about −10°C for Jarvis and King (1993) and −28°C for Bentley and Kohnen (1976). In agreement with previous laboratory measurements (Kuroiwa, 1964), we provide further field evidence that seismic attenuation in ice masses is significantly increased by raising ice temperature.

We observe that Q_P is lowered from 8 ± 1 to 5 ± 1 in the far-offset region of the seismic line. Since the wave propagates deeper at far offsets we interpret this variation by considering the ice-temperature profile with depth of our study area: far-offset arrivals sampled deeper, warmer and thus more attenuative ice. Consequently this technique seems to be sensitively dependent on ice temperature. Future developments, perhaps combined with radar surveys and by moving the shot position along the same seismic line, could offer new ways to detect the thermal state of ice masses.

The dependence of seismic attenuation on glacier-ice water content is still unclear. Quantitatively relating liquid water content and Q_P in temperate glacier ice is an exciting challenge for the future. We believe that introducing this methodology represents a valuable addition to characterizing glacier ice properties using in situ geophysical surveys. We hope that seismic Q_P estimates in glacier ice will become more common in reports of the hydrological and thermal characteristics of glaciers. Finally, we suggest that further combined application of radar and seismic techniques will enhance our understanding of ice rheology and contribute to continued improvements in ice-flow models.

ACKNOWLEDGEMENTS

A.G. is funded by a Swansea University postgraduate scholarship and Consorzio dei Comuni del Bacino Imbrifero Montano dell'Adda. A.D.B. is supported by the GLIMPSE project funded by the Leverhulme Trust. Fieldwork was funded by Swansea University and the Dudley Stamp Memorial Fund. R. Pettersson kindly provided temperature data, B. Reinardy helped with data acquisition and D. Hjelm gave field assistance. We thank P. Jansson, H. Törnberg, G. Rosquist and C. Helanow for the excellent logistics provided at the Tarfala Research Station. Queen's University in Belfast let us use their seismic system and C. Leech provided helpful advice about the seismic software. We thank L. Moffat, T. Blanchard and C. Reine for thoughtful discussions. This paper was significantly improved by the constructive reviews of the scientific editor M.T. Gudmundsson, F. Navarro and an anonymous reviewer.

REFERENCES

Aki, K. and P.G. Richards. 2002. *Quantative seismology. Second edition*. Sausalito, CA, University Science Books.

Barrett, B.E., T. Murray and R. Clark. 2007. Errors in radar CMP velocity estimates due to survey geometry, and their implication for ice water content estimation. *J. Environ. Eng. Geophys.*, **12**(1), 101–111.

Benjumea, B., Yu.Ya. Macheret, F.J. Navarro and T. Teixidó. 2003. Estimation of water content in a temperate glacier from radar and seismic sounding data. *Ann. Glaciol.*, **37**, 317–324.

Bentley, C.R. and H. Kohnen. 1976. Seismic refraction measurements of internal friction in Antarctic ice. *J. Geophys. Res.*, **81**(8), 1519–1526.

Bradford, J.H. and J.T. Harper. 2005. Wave field migration as a tool for estimating spatially continuous radar velocity and water content in glaciers. *Geophys. Res. Lett.*, **32**(8), L08502. (10.1029/2004GL021770.)

Bradford, J.H., J. Nichols, T.D. Mikesell and J.T. Harper. 2009. Continuous profiles of electromagnetic wave velocity and water content in glaciers: an example from Bench Glacier, Alaska, USA. *Ann. Glaciol.*, **50**(51), 1–9.

Chandler, D., B. Hubbard, A. Hubbard, T. Murray and D. Rippin. 2008. Optimising ice flow law parameters using borehole deformation measurements and numerical modelling. *Geophys. Res. Lett.*, **35**(12), L12502. (10.1029/2008GL033801.)

Clee, T.E., J.C. Savage and K.G. Neave. 1969. Internal friction in ice near its melting point. *J. Geophys. Res.*, **74**(4), 973–980.

Dasgupta, R. and R.A. Clark. 1998. Estimation of *Q* from surface seismic reflection data. *Geophysics*, **63**(6), 2120–2128.

Duval, P. 1977. The role of the water content on the creep rate of polycrystalline ice. *IAHS Publ.* 118 (Symposium at Grenoble 1975 – *Isotopes and Impurities in Snow and Ice*), 29–33.

Dvorkin, J. and A. Nur. 1993. Dynamic poroelasticity: a unified model with the squirt and the Biot mechanisms. *Geophysics*, **58**(4), 524–533.

Endres, A.L., T. Murray, A.D. Booth and L.J. West. 2009. A new framework for estimating englacial water content and pore geometry using combined radar and seismic wave velocities. *Geophys. Res. Lett.*, **36**(4), L04501. (10.1029/2008GL036876.)

Futterman, W.I. 1962. Dispersive body waves. *J. Geophys. Res.*, **67**(13), 5279–5291.

Gusmeroli, A., T. Murray, B. Barrett, R. Clark and A. Booth. 2008. Correspondence. Estimates of water content in glacier ice using vertical radar profiles: a modified interpretation for the temperate glacier Falljökull, Iceland. *J. Glaciol.*, **54**(188), 939–941.

Holmlund, P. and M. Eriksson. 1989. The cold surface layer on Storglaciären. *Geogr. Ann., Ser. A*, **71**(3–4), 241–244.

Hubbard, B.P., A. Hubbard, H.M. Mader, J.L. Tison, K. Grust and P.W. Nienow. 2003. Spatial variability in the water content and rheology of temperate glaciers: Glacier de Tsanfleuron, Switzerland. *Ann. Glaciol.*, **37**, 1–6.

Jarvis, E.P. and E.C. King. 1993. The seismic wavefield recorded on an Antarctic ice shelf. *J. Seism. Explor.*, **2**(1), 69–86.

Jeng, Y., J.-Y. Tsai and S.-H. Chen. 1999. An improved method of determining near-surface *Q*. *Geophysics*, **64**(5), 1608–1617.

Johnston, D.H., M.N. Toksöz and A. Timur. 1979. Attenuation of seismic waves in dry and saturated rocks: II. Mechanisms. *Geophysics,* **44**(4), 691–711.

King, E.C., A.M. Smith, T. Murray and G.W. Stuart. 2008. Glacier-bed characteristics of midtre Lovénbreen, Svalbard, from high-resolution seismic and radar surveying. *J. Glaciol.*, **54**(184), 145–156.

Kjartansson, E. 1979. Constant Q-wave propagation and attenuation. *J. Geophys. Res.*, **84**(B9), 4737–4748.

Knopoff, L. 1964. Q. *Rev. Geophys.*, **2**(4), 625–660.

Kuroiwa, D. 1964. Internal friction of ice. III. The internal friction of natural glacier ice. *Contrib. Inst. Low Temp. Sci., Ser. A* 18, 49–62.

Macheret, Yu.Ya. and A.F. Glazovsky. 2000. Estimation of absolute water content in Spitsbergen glaciers from radar sounding data. *Polar Res.*, **19**(2), 205–216.

Macheret, Yu.Ya., M.Yu. Moskalevsky and E.V. Vasilenko. 1993. Velocity of radio waves in glaciers as an indicator of their hydrothermal state, structure and regime. *J. Glaciol.*, **39**(132), 373–384.

Mitchell, B. 1975. Regional Rayleigh wave attenuation in North America. *J. Geophys. Res.*, **80**(35), 4904–4916.

Murray, T., G.W. Stuart, M. Fry, N.H. Gamble and M.D. Crabtree. 2000. Englacial water distribution in a temperate glacier from surface and borehole radar velocity analysis. *J. Glaciol.*, **46**(154), 389–398.

Murray, T., A. Booth and D.M. Rippin. 2007. Water-content of glacier-ice: limitations on estimates from velocity analysis of surface ground-penetrating radar surveys. *J. Environ. Eng. Geophys.*, **12**(1), 87–99.

Navarro, F.J., Yu.Ya. Macheret and B. Benjumea. 2005. Application of radar and seismic methods for the investigation of temperate glaciers. *J. Appl. Geophys.*, **57**(3), 193–211.

Peters, L.E., S. Anandakrishnan, C.W. Holland, H. Horgan, D.D. Blankenship and D.E. Voigt. 2008. Seismic detection of a subglacial lake near the South Pole, Antarctica. *Geophys. Res. Lett.*, **35**(23), L23501. (10.1029/2008GL035704.)

Pettersson, R., P. Jansson and P. Holmlund. 2003. Cold surface layer thinning on Storglaciären, Sweden, observed by repeated ground penetrating radar surveys. *J. Geophys. Res.*, **108**(F1), 6004. (10.1029/2003JF000024.)

Pettersson, R., P. Jansson and H. Blatter. 2004. Spatial variability in water content at the cold–temperate transition surface of the polythermal Storglaciären, Sweden. *J. Geophys. Res.*, **109**(F2), F02009. (10.1029/2003JF000110.)

Pohjola, V.A. 1994. TV-video observations of englacial voids in Storglaciären, Sweden. *J. Glaciol.*, **40**(135), 231–240.

Reine, C., M. van der Baan and R. Clark. 2009. The robustness of seismic attenuation measurements using fixed- and variable-window time-frequency transforms. *Geophysics*, **74**(2), WA123–WA135.

Reynolds, J.M. 1981. The distribution of mean annual temperatures in the Antarctic Peninsula. *Br. Antarct. Surv. Bull.* 54, 123–133.

Robin, G.de Q. 1958. Glaciology III. Seismic shooting and related investigations. *Norwegian–British–Swedish Antarctic Expedition, 1949–52, Scientific Results*, **5**. Oslo, Norsk Polarinstitutt.

Sams, M.S., J.P. Neep, M.H. Worthington and M.S. King. 1997. The measurement of velocity dispersion and frequency-dependent intrinsic attenuation in sedimentary rocks. *Geophysics*, **62**(5), 1456–1464.

Sheriff, R.E. and L.P. Geldart. 1995. *Exploration seismology. Second edition*. Cambridge, Cambridge University Press.

Smith, A.M. 1997. Basal conditions on Rutford Ice Stream, West Antarctica from seismic observations. *J. Geophys. Res.*, **102**(B1), 543–552.

Smith, A.M. 2007. Subglacial bed properties from normal-incidence seismic reflection data. *J. Environ. Eng. Geophys.*, **12**(1), 3–13.

Spencer, T.W., J.R. Sonnad and T.M. Butler. 1982. Seismic *Q* – stratigraphy or dissipation. *Geophysics*, **47**(1), 16–24.

Spetzler, H. and D. Anderson. 1968. The effect of temperature and partial melting on velocity and attenuation in a simple binary system. *J. Geophys. Res.*, **73**(18), 6051–6060.

Spetzler, J. and R. Snieder. 2004. The Fresnel volume and transmitted waves. *Geophysics*, **69**(3), 653–663.

Toksöz, M.N. and D.H. Johnston, *eds*. 1981. *Seismic wave attenuation*. Tulsa, OK, Society of Exploration Geophysicists. (Geophysics Reprint Series 2.)

Toksöz, M.N., D.H. Johnston and A. Timur. 1979. Attenuation of seismic waves in dry and saturated rocks: I. Laboratory measurements. *Geophysics*, **44**(4), 681–690.

Toms, J., T.M. Mller and B. Gurevich. 2007. Seismic attenuation in porous rocks with random patchy saturation. *Geophys. Prospect.*, **55**(5), 671–678.

Tonn, R. 1991. The determination of the seismic quality factor Q from VSP data: a comparison of different computational methods. *Geophys. Prospect.*, **39**(1), 1–27.

Topping, J. 1972. *Errors of observation and their treatment. Fourth edition*. London, Chapman and Hall.

Vaughan, D.G. and C.S.M. Doake. 1996. Recent atmospheric warming and retreat of ice shelves on the Antarctic Peninsula. *Nature*, **379**(6563), 328–331.

Wang, Y. 2003. Quantifying the effectiveness of stabilized inverse *Q* filtering. *Geophysics*, **68**(1), 337–345.

Westphal, J. 1965. In situ acoustic attenuation measurements in glacial ice. *J. Geophys. Res.*, **70**(8), 1849–1853.

Winkler, K.W. and A. Nur. 1982. Seismic attenuation: effects of pore fluids and frictional-sliding. *Geophysics*, **47**(1), 1–15.

Xia, J., R.D. Miller, C.B. Park and G. Tian. 2002. Determining *Q* of near-surface materials from Rayleigh waves. *J. Appl. Geophys.*, **51**(2–4), 121–129.

MS received 17 June 2009 and accepted in revised form 23 January 2010